MODE-MIXITY IN BEAM-LIKE GEOMETRIES: LINEAR ELASTIC CASES AND LOCAL PARTITIONING

B.R.K. Blackman[1], M. Conroy[2], A. Ivankovic[2], A. Karac[3], A. J. Kinloch[1], J. G. Williams[1]

[1] Department of Mechanical Engineering, Imperial College London, London SW7 2AZ, UK
[2]UCD School of Mechanical and Materials Engineering, UCD, Belfield, Dublin 4, Ireland
[3]Faculty of Mechanical Engineering, Fakultetska 1, Zenica, Bosnia and Herzegovina
*alojz.ivankovic@ucd.ie

Keywords: mixed-mode fracture, analytical solution, numerical simulation, ESIS TC4

Abstract
This work is conducted as a part of a wider international activity on mixed mode fractures in beam-like geometries under the coordination of European Structural Integrity Society, Technical Committee 4. In its initial phase, it considers asymmetric double cantilever beam geometry made of a linear elastic material with varying lower arm thickness and constant bending moment applied to the upper arm of the beam. A number of relevant analytical solutions are reviewed including classical Hutchinson and Suo local and Williams global partitioning solutions. Some more recent attempts by Williams, and Wang and Harvey to reproduce local partitioning results by averaging global solutions are also presented. Numerical simulations are conducted using Abaqus package. Mode-mixity is calculated by employing virtual crack closure technique and interaction domain integral. Both approaches gave similar results and close to the Hutchinson and Suo. This is expected as in this initial phase numerical results are based on local partitioning in an elastic material which does not allow for any damage development in front of the crack tip.

1 Introduction
Current fracture tests on composite laminates and composite adhesive joints make extensive use of beam-like geometries such as double cantilever beam (DCB), asymmetric DCB (ADCB), fixed ratio mixed-mode (FRMM), end loaded split (ELS), etc. Different mode-mixities can be obtained using different test configurations with beam arms of the same thickness: with $G_I/G=1$ using DCB, $G_I/G_{II}=4/3$ using FRMM, and $G_{II}/G=1$ using ELS, or by varying the arms thickness in an ADCB configuration. Here G_I, G_{II} and $G=G_I+G_{II}$ stand for mode I, mode II and total fracture energy, respectively. The tests are normally analysed using analytical or numerical methods, each of which suffers from a number of uncertainties.

The present work attempts to shed some light on both analytical and numerical approaches and ultimately develop a testing protocol and recommendations for the accurate determination of mode-mixity in beam-like geometries. At this initial stage, only linear elastic ADCB geometry is considered.

2 Analytical solutions

The problem to be analysed is shown in a general form in Fig.1. The total energy release rate may be computed exactly from

$$\frac{G}{G_1} = X_3 - 2k + X_4 k^2 \tag{1}$$

where $X_3 = (1+\gamma)^3 - 1$, $X_4 = \left((1+\gamma)/\gamma\right)^3 - 1$, $\gamma = h_2 / h_1$ and $G_1 = 6M_1^2 / \left(Eb^2 h^3\right)$.

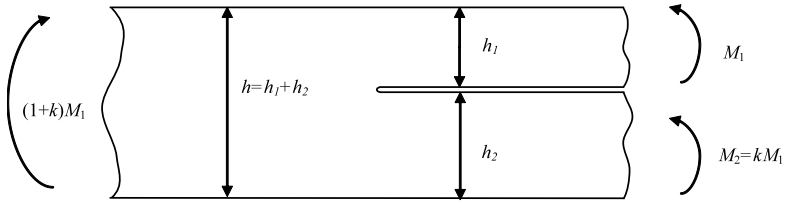

Figure 1. Loading and geometry

G may be partitioned into mode I and II by means of M_I and M_{II}, the moments contributions for each mode, such that

$$\begin{aligned} M_1 &= M_I + M_{II} \\ kM_1 &= -\lambda_2 M_I + \lambda_1 M_{II} \end{aligned} \tag{2}$$

where $\lambda_{1,2}$ are functions of γ. Thus, G_I and G_{II} may be found from M_I and M_{II}, respectively, as

$$\begin{aligned} \frac{G_I}{G_1} &= \left[X_3 + \lambda_2^2 X_4 + 2\lambda_2\right]\left(\frac{\lambda_1}{\lambda_1+\lambda_2}\right)^2\left(1-\frac{k}{\lambda_1}\right)^2 \\ \frac{G_{II}}{G_1} &= \left[X_3 + \lambda_1^2 X_4 - 2\lambda_1\right]\left(\frac{\lambda_2}{\lambda_1+\lambda_2}\right)^2\left(1+\frac{k}{\lambda_2}\right)^2 \end{aligned} \tag{3}$$

There are two unknowns, λ_1 and λ_2 and one condition, i.e. $G_I+G_{II}=G$, which gives

$$X_3 - X_4\lambda_1\lambda_2 - (\lambda_1 - \lambda_2) = 0 \tag{4}$$

For the symmetric case of $\gamma = 1$ we have, $X_3 = X_4 = 7$ and $\lambda_1 = \lambda_2 = 1$, and exact solutions; for $k = 0$, i.e. the lower arm is not loaded, $G_I / G = 4/7$ and $G_{II} / G = 3/7$. For $\gamma \neq 1$ there are no exact solutions and the mode partition depends on the stress state at the crack tip. For a purely elastic state there is singular stress field near the crack tip whilst in cases where damage (cohesive) zone of finite size develops in front of the crack tip this singularity is removed, either partly or completely.

2.1 The Williams solution

The form of the solution may be determined from the observation that for no crack opening (mode II) $\lambda_1 = \gamma^3$ and for no sliding on the crack face (mode I) $\lambda_2 = \gamma^2$. This pair does not satisfy Eq. (4) and results in two following pairs

$$\begin{aligned} &\lambda_1 = \gamma^3, \quad \lambda_2 = 1 \\ &\lambda_1 = \gamma^2\left(\frac{3+\gamma}{1+3\gamma}\right), \quad \lambda_2 = \gamma^2 \end{aligned} \tag{5}$$

The first pair represents the Williams pair [1] or the upper-bound solution (W-UB), with

$$G_I = \frac{\gamma^3(1+\gamma)^3}{1+\gamma^3}G_1, \qquad G_{II} = \frac{3\gamma(1+\gamma)}{1+\gamma^3}G_1 \tag{6}$$

The second pair represents the Wang and Harvey pair [2-4] (see Section 2.3), which with Equation (3) produces lower bound solution (W/WH-LB)

$$G_I = \frac{1}{4}\gamma(3+\gamma)^2 G_1, \qquad G_{II} = \frac{3}{4}\gamma(1+\gamma)^2 G_1 \tag{7}$$

2.2 The Hutchinson-Suo solution

Hutchinson and Suo (H&S) partitioned the fracture energy using analytical expressions for mixed-mode intensity factors with numerically calculated and then linearly approximated parameter ω [5]. Their solution here, however, is shown in form of Equation (3) with following values for λ_1 and λ_2 (W-H&S)

$$\lambda_1 = \frac{\gamma^2(3+3\gamma+\gamma^2)}{\gamma+\sqrt{3\varphi}(1+\gamma)^2}, \quad \lambda_2 = \frac{\varphi\cdot\gamma^2(3+3\gamma+\gamma^2)}{\sqrt{3\varphi}(1+\gamma)^2-\varphi\cdot\gamma} \tag{8}$$

and parameter φ being an approximation of parameter $\omega = 52.1° - 3°/\gamma$ in the following form

$$\varphi \approx \frac{3}{4}\left(1-0.2\cdot\left(\frac{\gamma-1}{\gamma}\right)\right) \tag{9}$$

It has to be noted that Equations (8) and (9) are valid for $1<\gamma<\infty$ only, but can be adapted to account for $0<\gamma<1$ as well. For this range, one should use $1/\gamma$ instead of γ in Equation (9) and swap λ_1 and λ_2, Equation (8), when using Equation (3).

2.3 The Wang-Harvey solutions

Wang and Harvey applied both pairs of Equation (5) to Euler and Timoshenko beam theories. Timoshenko partition rule, with no interactions between mode I and Mode II (pairs in Equation (5) coincide), recovered lower bound solution (Equation (7)). On the other hand, in Euler beam theory crack tip shear force has to be taken into account, discovering stealthy interaction between pure modes. As a result, the lower bound solution is modified to account

for interaction between pure modes, leading to the Wang and Harvey upper bound solution (W&H-UB). More details can be found in [2-4] with following final values for mixed modes:

$$G_I = \gamma^2 (3+\gamma) G_1, \qquad G_{II} = 3\gamma G_1 \tag{10}$$

In their work [2-4], Wang *et.al.* also proposed the averaged partition rule (W&H-avg) where the lower and their upper bound solutions are averaged, leading to the following mixed modes

$$G_I = \frac{1}{8}\gamma (3+5\gamma)(3+\gamma) G_1, \qquad G_{II} = \frac{3}{8}\gamma (5+2\gamma+\gamma^2) G_1 \tag{11}$$

2.4 The Williams average solution (W-avg)

It is proposed here that an average of two pairs in Equation (3) must be generated depending on the size of the singular zone present and that this can be defined for the $k = 0$ and $\gamma \to \infty$ case, leading to the upper, ie. $(G_I/G)_\infty=1$, and lower, ie. $(G_I/G)_\infty=0.25$, bounds and intermediate value given by

$$\left(\frac{G_I}{G}\right)_\infty = f + (1-f)\frac{1}{4} = \frac{1+3f}{4} \tag{12}$$

For the singular case f=0.5, i.e. equal sharing, and $(G_I/G)_\infty = 5/8$ and for no singular field, f = 1 and $(G_I/G)_\infty = 1$, pure mode I. Intermediate values are deduced by interpolation between $\gamma = 1$ and ∞ by the parameter n defined as

$$n = \frac{(\lambda_1 - \lambda_2)\gamma^2}{(\gamma^3 - \lambda_1\lambda_2)} \qquad \left(\text{from } \frac{\lambda_1}{\gamma^2} = \frac{n + \lambda_2/\gamma^2}{1 + n\lambda_2/\gamma^2}\right) \tag{13}$$

Substituting equation (13) into equation (4) gives two equations

$$\left[1 + (3-n)\gamma + 3\gamma^2\right]\left(\frac{\lambda_{1,2}}{\gamma^2}\right)^2 \pm 2n(\gamma^2 - 1)\left(\frac{\lambda_{1,2}}{\gamma^2}\right) - \left[3 + (3-n)\gamma + \gamma^2\right] = 0 \tag{14}$$

with '+' for λ_1 and '–' for $\lambda 2$. Using Equation (14) as $\gamma \to \infty$, one can recover relationship between f and n as

$$n^2 = \frac{3(3f-1)^2}{4 - (3f-1)^2} \tag{15}$$

and for $f = 1$, $n \to \infty$ and for f=0.5, $n = 1/\sqrt{5}$. For any f value n may be found from Equation (15), and for each γ value λ_1 and λ_2 found from Equation (14). These are then used with Eq. (3) to obtain G_I and G_{II}.

3 Numerical solutions

Two post processing methods were used to predict the mode mixity for the 2D plain strain problem posed in Fig.1. The length of the beam was 120 mm with 60 mm precrack length and

in this purely elastic case, the crack initiation and propagation are not considered. Bending moment was applied to the upper arm only (k=0), and the numerical simulations were carried out using the commercial software Abaqus. All simulations, unless otherwise stated, use a structured orthogonal mesh with quadratic, plain strain, CPE4 elements. The width t, of the sample was kept constant at 1 m. To achieve varying h_1/h_2 ratios, h_1 was kept constant at 3mm while h_2 was varied between 0.3, 0.6, 1.5, 3, 6, 15,& 30mm. The two techniques used to numerically calculate the mode I and mode II energy release rates were the *Virtual crack closure technique* (VCCT) [6] and *Interaction domain integral* (IDI) [7,8].

3.1 The VCCT technique

This method, as described in [6], uses global nodal forces, $F^{(g)}$, ahead of the crack tip and the differences in the vertical and horizontal nodal displacements, $\Delta v_n, \Delta u_n$, behind the crack tip to calculate the individual energy release rates. Below are the VCCT formulae used for the case of quadratic elements with mid side nodes.

$$G_I = \frac{1}{2t\Delta a}\left(\Delta v_2 F_{y,2'}^{(g)} + \Delta v_3 F_{y,3'}^{(g)}\right)$$
$$G_{II} = \frac{1}{2t\Delta a}\left(\Delta u_2 F_{x,2'}^{(g)} + \Delta u_3 F_{x,3'}^{(g)}\right) \tag{16}$$

where each term is explained in Fig. 2. This method was implemented manually for each case using the relevant Abaqus outputs of global nodal force and nodal displacements.

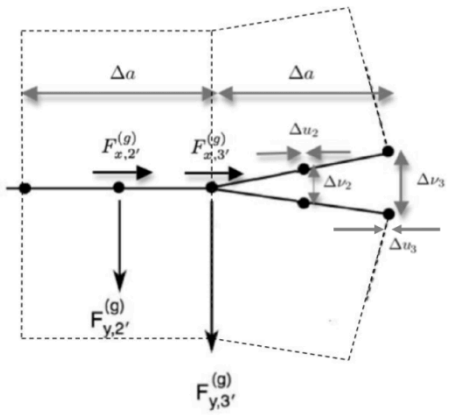

Figure 2 *VCCT technique* [6]

3.2 The IDI technique

This method, which is described in more detail in [7,8], is pre-implemented within the Abaqus code. The method imposes an auxiliary field (superscript (2)) of known singular solution on to the actual mixed mode field (superscript (1)) which results in a new field (superscript (0)). The J integral of this new field can be expressed as

$$J^{(0)} = J^{(1)} + J^{(2)} + M^{(1,2)} \tag{17}$$

where $M^{(1,2)}$ is known as the interaction integral and can be evaluated as a domain integral

$$M^{(1,2)} = \sum_{A} \sum_{p=1}^{N} \left\{ \left[-w^{(1,2)} \delta_{1j} + \sigma_{ij}^{(1)} \frac{du_i^{(2)}}{dx} + \sigma_{ij}^{(2)} \frac{du_i^{(1)}}{dx} \right] \frac{dq}{dx_i} \det\left(\frac{dx_k}{d\eta_j} \right) \right\} w_p \tag{18}$$

where N is the number of Gaussian points within each element in domain A and w_p are the corresponding weights associated with each Gaussian point. q is an arbitrary continuous scalar function which varies from a value of 1 at the crack tip to a value of 0 at the domain boundaries. All quantities inside braces {} are evaluated at the individual Gaussian points. $w^{(1,2)}$ is the mutual potential energy density defined by

$$w^{(1,2)} = \sigma_{ij}^{(1)} \varepsilon_{ij}^{(2)} = \sigma_{ij}^{(2)} \varepsilon_{ij}^{(1)} \tag{19}$$

It can be shown that

$$M^{(1,2)} = \frac{2}{E'} (K_I^{(1)} K_I^{(2)} + K_{II}^{(1)} K_{II}^{(2)}) \tag{20}$$

Therefore, if the auxiliary singular field (2) is chosen such that $K_I^{(2)} = 1; K_{II}^{(2)} = 0,$ it is possible to calculate $K_I^{(1)}$ from Eq. (19) and if the auxiliary field is chosen such that $K_I^{(2)} = 0; K_{II}^{(2)} = 1,$ it is then possible to evaluate $K_{II}^{(1)}$. The individual energy release rates of the actual field can then be evaluated using

$$G_I = \frac{1}{E'} (K_I^{(1)})^2; G_{II} = \frac{1}{E'} (K_{II}^{(1)})^2 \tag{21}$$

4 Results

The analytically and numerically obtained values of G_I/G are presented in Fig.3 for each configuration of h_1/h_2. It can be seen that only averaged solutions (W-avg and W&H-avg) are close to Hutchinson and Suo (H&S and W-H&S) and numerical predictions; other solutions, representing lower and upper bounds, cannot be used to predict this type of problem. On the other hand, the numerical solution is very close for both the VCCT and IDI methods. The values quoted for G_I/G for both the VCCT and IDI methods are obtained by extrapolating convergence trend-lines to zero (see Section 4.1). It is interesting that this solution always lies between that of Hutchinson and Suo and averaged solutions. Also worth noting is that the result of Hutchinson and Suo cannot be taken as exact as it also requires numerical calculations which can lead to possible errors of 1% [9].

4.1 Convergence of VCCT and IDI methods

The convergence trend-lines shown in Fig.4a highlight some interesting properties of both the VCCT and IDI methods. Surprisingly the values of G_I/G, by VCCT method, do not monotonically converge. For each case of $h_1/h_2 > 1$, G_I/G reaches a maximum and then starts to decrease as the mesh is further refined. Contrary to this, when $h_1/h_2 < 1$, G_I/G reaches a minimum and then begins to increase as the mesh is further refined. This behaviour was first reported by Nairn [9] and it is verified here. It was found that a best fit quadratic equation excellently approximates the VCCT convergence pattern and it was therefore used to obtain the extrapolated values.

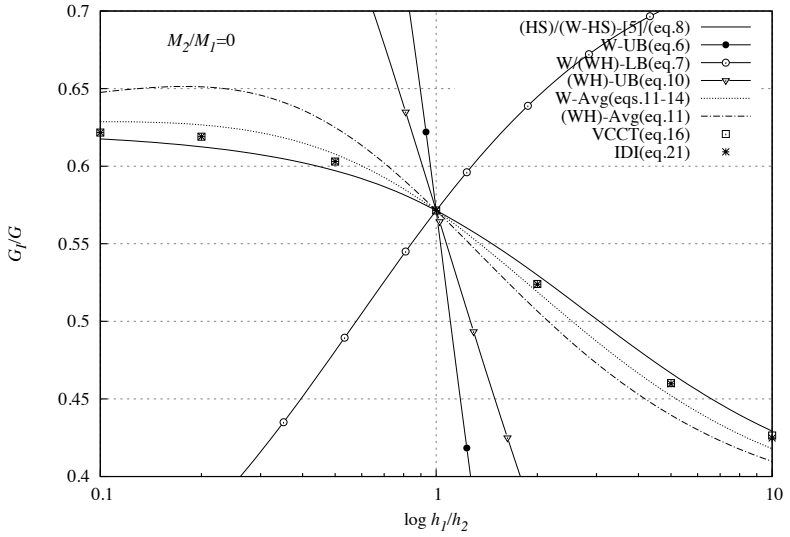

Figure 3. *Plot of G_I/G vs. h_1/h_2 for all numerical and analytical solutions*

On the other hand, the IDI method does show clear linear monotonic convergence for each case of h_1/h_2. Figure 4b shows a representative close up of the convergence pattern for each method. Note that the convergence of two IDI methods, namely, regular and singular, refer to the type of mesh used in the crack tip region. Abaqus documentation [10] recommends that collapsed singular elements are used at the crack tip in order to obtain the most accurate results from the IDI method. This is indeed verified as shown in Fig. 4b and it also highlights that the IDI method applied to a regular orthogonal mesh will only be accurate if convergence tests with extrapolation to zero are carried out.

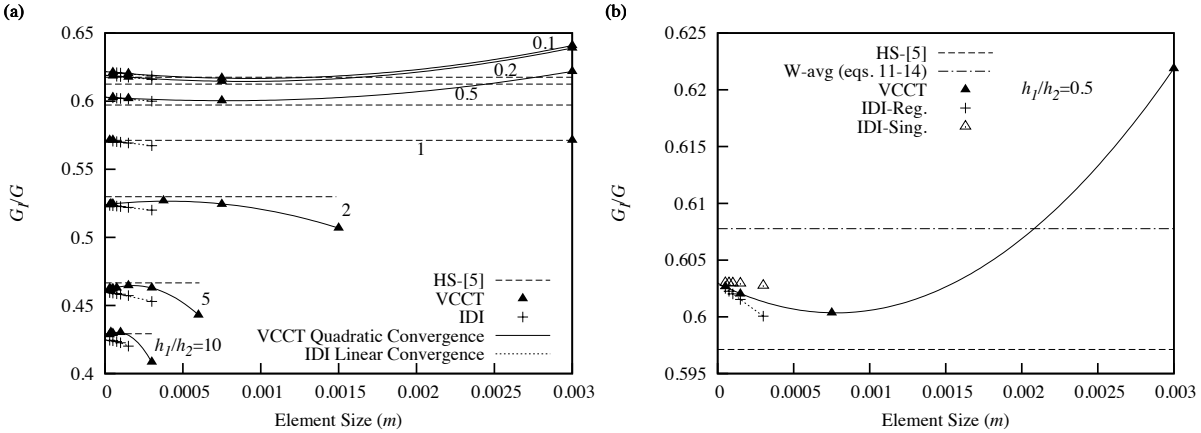

Figure 4. *Convergence of VCCT and IDI methods:* **(a)** *for each h_1/h_2.* **(b)** *for h_1/h_2=0.5.*

For all cases, the IDI method predicted G with very good accuracy (max error <0.02 %). For h_1/h_2<1, the VCCT method predicted G very accurately even for coarse meshes (max error < 0.01%). However, for h_1/h_2>1 VCCT convergence curves exhibit irregular, oscillatory patterns which resulted in increasing inaccuracy of G as the mesh was refined, see Fig. 5b, which also lead to minor deviations from the quadratic convergence pattern of G_I/G, see Fig. 5a. Arguably, the irregular convergence patterns might be caused by inability of the numerical solutions to accurately predict high gradients very close to the crack tip. Interestingly, this erratic behaviour when h_1/h_2>1 was not reported in [9] where similar tests were carried out using the finite element software NairnFEA. Further investigations will be carried out to determine the exact cause of this behaviour.

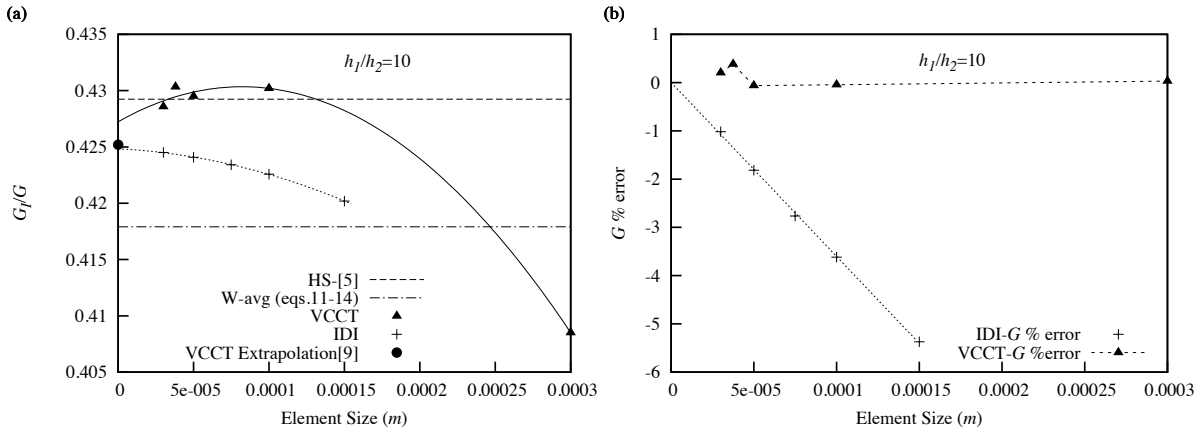

Figure 5. *h_1/h_2=10 analysis:* **(a)** *Convergence of VCCT and IDI methods*. **(b)** *G % Error plot*

5 Conclusions

Numerical results on mode partitioning in elastic ADCB geometry closely followed Hutchinson and Suo local predictions. This is as expected since the simulations did not allow any damage development in the specimens and hence the singular field was preserved in the crack tip region. Small differences between numerical and analytical results may be attributed to the fact that Hutchinson and Suo solution is not exact (involves numerically calculated and then linearly approximated parameter (ω) and also to numerical extrapolations to zero element size. Averaged Williams, and Wang and Harvey solutions were found to be reasonable approximation of Hutchinson and Suo solution. Both VCCT and IDI techniques produced accurate results. While VCCT is simpler to implement it was found to experience irregular convergence behaviour unlike IDI. As real experiments deal with real materials, the next phase of the work will focus on simulations involving damage development.

References

[1] Williams JG. On the calculation of energy release rates for cracked laminates. *International Journal of Fracture Mechanics*, **36,** pp. 101-119 (1988).

[2] S. Wang, L. Guan, On fracture mode partition theories, *Computational Material Science*, **52**, pp. 240-245 (2012).

[3] S. Wang, C.M. Harvey, Mixed mode partition theories for one dimensional fracture, *Engineering Fracture Mechanics*, **79**, pp. 329-352 (2012).

[4] C.M. Harvey, S. Wang, Experimental assessment of mixed-mode partition theories, *Composie Structures*, **96**, pp. 758-767 (2012).

[5] J.W. Hutchinson, Z. Suo. Mixed Mode Cracking in Layered Materials, *Advances in Applied Mechanics*, **29**, pp. 63-191 (1992).

[6] Nairn J.A., Generalized Crack Closure Analysis for Elements with Arbitrarily-Placed Side Nodes and Consistent Nodal Forces. *International Journal of Fracture,* **171**, pp. 11-22 (2011)**.**

[7] Yau J.F., Wang S.S., A mixed-mode crack analysis of isotropic solids using conservation laws of elasticity. *International Journal of Fracture*, **47**, pp. 335-340 (1980).

[8] Shih C. F. and Asaro R. J., Elastic-Plastic Analysis of Cracks on Bimaterial Interfaces: Part I-Small Scale Yielding, *Journal of Applied Mechanics*, **55**, pp. 299–316 (1988).

[9] Nairn J.A., ESIS TC4 Mixed Mode Round Robin Phase 1 Report (2011).

[10] Abaqus Theory Manual V.6.9. Dassault Systèmes (2009).